JOURNAL OF PROPULSION AND POWER
Vol. 22, No. 4, July–August 2006

Numerical Analysis of Free-Molecule Microresistojet Performance

Zeeshan Ahmed* and Sergey F. Gimelshein†
University of Southern California, Los Angeles, California 90089
and
Andrew D. Ketsdever‡
U.S. Air Force Research Laboratory, Edwards Air Force Base, California 93524

The direct-simulation Monte Carlo method was used to study the flow in a free-molecule microresistojet (FMMR). The FMMR is a microelectromechanical-systems (MEMS) fabricated resistojet that operates by heating a propellant gas as it expands through a series of slots. The flow through a single heater slot of the FMMR was modeled in two dimensions for a range of chamber pressures from 50 to 200 Pa and heater chip temperatures from 300 to 573 K. Using this, the numerical performance of FMMR was computed. The resultant specific impulse was found to agree within 2% of experimental data for nitrogen propellant and within 4% for helium propellant. Then, a full three-dimensional model of the FMMR geometry was made for water vapor as propellant in two steps. First, the flow in the plenum was modeled. FMMR performance parameters were found to be 10% lower than those of the two-dimensional model. Second, the FMMR plume flow was calculated using a starting surface generated from the plenum simulation for two possible locations of the FMMR as a despin thruster on a nanosatellite. The thrust degradation caused by the resultant surface forces was examined, and the net moment of one configuration was found to be 60% higher than the other.

I. Introduction

ONE of the increasing trends in the design of modern space missions is the miniaturization of spacecraft and satellites. As a result, new space technologies, such as spacecraft formation flying, have been promoted by the U.S. Air Force, Defense Advanced Research Projects Agency, and NASA. The growing emphasis on small satellite systems necessitates the development of new propulsion systems able to deliver precise impulse bits while meeting strict mass, size, and power usage limitations.[1]

Various micropropulsion concepts, such as cold gas,[2] catalytic decomposition,[3] mono-propellant, and bipropellant[4] thrusters, are currently being considered for small satellite applications. For chemical and electrothermal micropropulsion devices, the fluid mechanics of reduced length scales (low Reynolds numbers) results in a significant degradation of the thrust efficiency as a result of increased viscous and heat-transfer losses. Both experimental and numerical investigation of fluid flow and performance of microthrusters is necessary for realistic evaluation of new concepts.

The free-molecule microresistojet (FMMR) is an electrothermal propulsion system designed for on-orbit maneuvers of nanospacecraft (mass < 10 kg) (Refs. 5 and 6). The current version of the FMMR[6] is being developed for a Texas A&M (TAM) nanosatellite flight. The flight will investigate the survivability and capability of the water-propelled microthruster for attitude control maneuvers. The FMMR will provide a spin-up capability for the nanosatellite. The thruster system will operate on the vapor pressure of water, stored in either a liquid or solid state (depending on the internal satellite temperature). The propellant gas, originating from a propellant tank and passing through hydrophobic microporous membrane filters and a valve, enters the base of a Teflon® plenum through an inlet. The hydrophobic microporous membrane uses the surface tension of the propellant to serve as a phase separator, allowing only the propellant vapor to pass through. The FMMR heater chip shown in Fig. 1 is attached to the top of the plenum. Propellant molecules gain kinetic energy as they collide with heated walls of the expansion slots. The increase in kinetic energy of the propellant molecules is critical to the performance and operation of the FMMR. Because of the inherently low operating pressures of the FMMR, the propellant molecules are heated primarily through the direct interaction with the expansion slots.[5]

The FMMR exhibits many systemic features that are beneficial to small satellite operations such as low cost, low power consumption, low mass, and low propellant storage volume. The FMMR operates at relatively low stagnation pressure to take advantage of the high storage density of liquid and solid propellants. By operating on the vapor pressure of the stored propellant, the FMMR reduces the amount of power required over thrusters that prevaporize the propellant to create high stagnation pressures. The simple design of the FMMR allows for low-cost manufacturing and testing. The FMMR heater chip allows for large ranges of thrust levels without a significant loss in performance by varying the number and dimensions of the expansion slots.

Previous work has described the fabrication and heat-transfer characteristics of the FMMR concept.[5] Proof-of-principle designs, which showed the utility of the FMMR system for nanosatellite operations, were investigated. Analytical expressions were developed to estimate the overall propulsive efficiency of the design. Recently, the propulsive performance of the FMMR has been determined experimentally.[6] Comparison of the experimental performance data with the analytical results showed that the design of the FMMR based on these free-molecule analytical expressions has met with limited success. The range of operating pressures of the FMMR propulsion system extends into the transitional flow regime where the free-molecule analytical expressions are not completely valid. In Ref. 6, the analytically predicted specific impulse is shown to be up to 20% lower than experimental measurements. Therefore, the need for higher accuracy performance predictions for designing future iterations of the FMMR is evident. In this work, a FMMR is examined numerically. Because typical plenum pressures

Presented as Paper 2005-4262 at the AIAA/ASME/SAE/ASEE 41st Joint Propulsion Conference and Exhibit, Tucson, AZ, 10–13 July 2005; received 19 August 2005; revision received 9 December 2005; accepted for publication 12 January 2006.

*Undergraduate Student.
†Research Assistant Professor.
‡Group Leader, Nonequilibrium Flows Group, Propulsion Directorate.

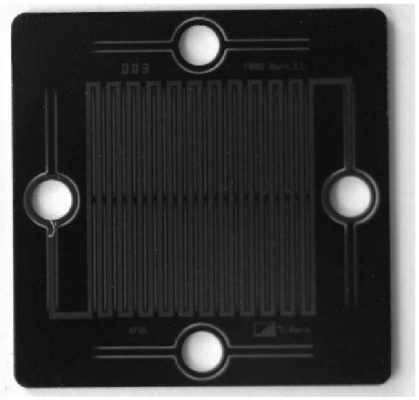

a)

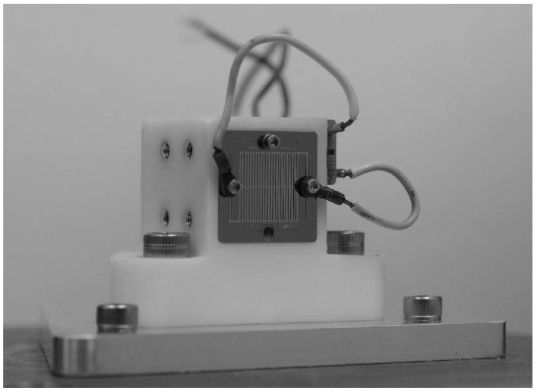

b)

Fig. 1 MEMS fabricated resistojet: a) FMMR heater chip and b) the plenum with the mounted heater chip.

are relatively low (below 1000 Pa) and the Knudsen number based on the slot thickness is on the order of unity, the direct simulation Monte Carlo (DSMC) method has been used in all computations in this study.

The main objectives of this work were threefold. First, the performance of the FMMR was compared to experimental data for different test gases to validate the use of the numerical model and provide a level of confidence in extending the model to simulate performance on the TAM nanosatellite. The second objective was to use the validated code to estimate the level of contamination of a typical spacecraft surface by propellant molecules. Because experimental contamination data are not available, DSMC provides the only means to predict the contamination potential on the TAM nanosatellite. Finally, an analysis of the importance of geometrical and operational parameters, such as plenum pressures and heater chip temperatures, was performed. This final objective was used to investigate the potential of the DSMC technique as a design tool for future iterations of the FMMR system. For initial design criteria, the derived free-molecule analytical expressions given in previous studies[5,6] were utilized. The analytical expressions are valid for low-pressure (high Knudsen number) operation of the thruster but are not expected to be accurate for the higher operating pressure range. Furthermore, future design iterations of the FMMR system will require higher accuracy performance predictions, which might eventually couple the heat-transfer and gas dynamic effects. DSMC offers the opportunity to accurately predict FMMR performance throughout the design process over a wide range of operating parameters.

II. Geometry and Flow Conditions

The current iteration of the FMMR heater chip, shown in Fig. 1a, was designed specifically for the TAM nanosatellite mission. This iteration of the FMMR chip is an 19.2×19.2 mm square with a thickness L of 500 μm. There are 44 interior expansion slots formed in two rows. Each slot is 100 μm wide by 5.375 mm long and is etched completely through the FMMR. The expansion slots are outlined by a serpentine heater pattern consisting of a gold current carrying layer.

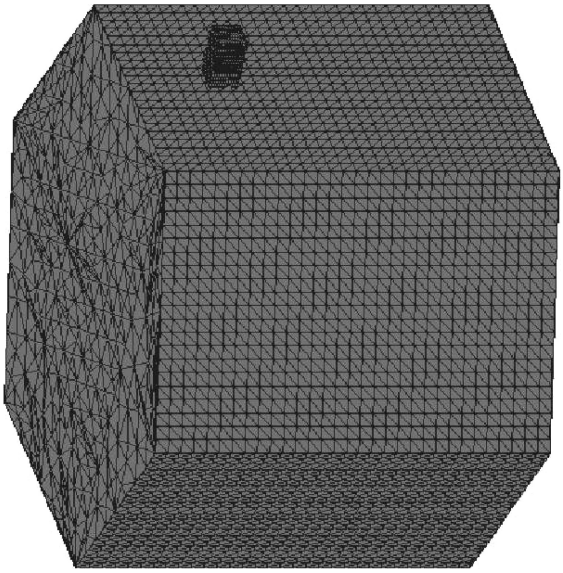

Fig. 2 Satellite geometry.

The plenum is designed as a rectangular box as shown in Fig. 1b. The internal dimensions of the plenum are $11 \times 11 \times 22$ mm. The propellant gas is flowing through the attached tube of 6.35 mm diam, and the plenum pressure can vary from tens to hundreds of Pascals. Although the heater chip temperature will be kept at about 573 K, the temperature of other walls of the plenum will be close to room temperature.

The current design of the satellite represents a 316-mm-long hexagonal cylinder with a side width of 216 mm. The FMMR thruster is mounted on one of the plates of the hexagonal cylinder surface as shown in Fig. 2. The figure also illustrates the triangulated geometry used in the computations.

III. Numerical Approach

The DSMC-based software system SMILE[7] was used in computations. The majorant frequency scheme[8] was used to calculate intermolecular interactions. The intermolecular potential was assumed to be a variable hard sphere.[9] Energy redistribution between the rotational and translational modes was performed in accordance with the Larsen–Borgnakke model. A temperature-dependent rotational relaxation number was used. The reflection of molecules on the surface was assumed to be diffuse with complete energy accommodation.

To examine the flow details inside the plenum, near the expansion slots, as well as in the plume interacting with the spacecraft surface, the computations have been performed in three steps. The first step is the DSMC modeling of a two-dimensional flow through a single expansion slot. The etching technology used in FMMR manufacturing results in a slot geometry that is not rectangular. Therefore, the actual geometry of the slot was evaluated from the scanning electron microscope (SEM) data. (The schematic of the geometry is shown in Fig. 3.) The detailed modeling of the gas flow through a single slot allows for comparison of computed mass flow and thrust with available experimental data[10] for helium and nitrogen propellants. The computations are also performed for water vapor. The second step includes three-dimensional modeling of the water vapor flow inside the plenum and in a small region outside of the FMMR (near field of the plume). The complex geometry of the slots is replaced by rectangular openings described in the preceding section. The third step is the modeling of the plume flow and plume impingement on spacecraft surfaces. A starting surface is generated using the macroparameters obtained at the previous step. The starting surface specifies inflow boundary conditions used for the

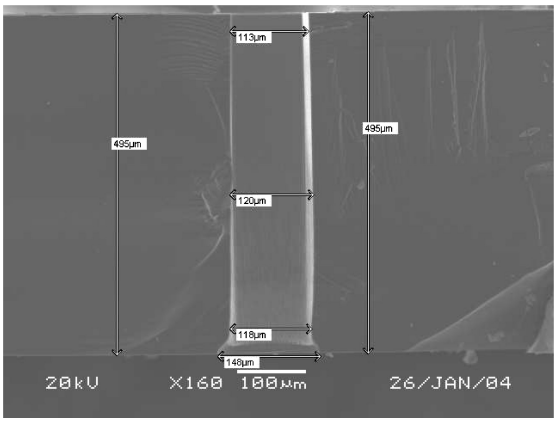

Fig. 3 SEM image of a single slot of FMMR (right).

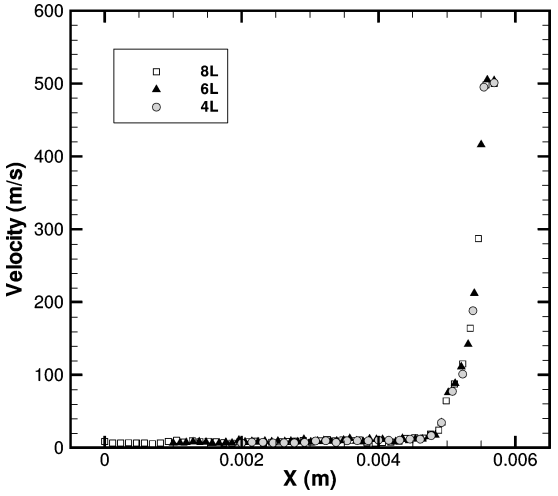

Fig. 4 Axial-velocity profile along the axis of symmetry for different computational domains.

plume impingement modeling step. The surface is 2×2 cm and is located 0.5 mm downstream from the heater chip plane. The inflow molecules are introduced from the starting surface with parameters calculated at the second step; the molecules are sampled from the corresponding ellipsoidal[11] distribution functions. The use of the ellipsoidal distribution function is important because there is a significant, up to a factor of two, difference in temperatures in the directions parallel and perpendicular to the plume.

The DSMC method is conventionally used to model supersonic and hypersonic flows where the boundary conditions are either supersonic inflow or vacuum outflow. For subsonic flows, such as the flow inside the plenum, the application of the DSMC method is more complicated. In the present study, the convergence study has been conducted in order to establish the minimum necessary size of the computational domain. Note that for all two-dimensional computations zero flow velocity was assumed at the inflow boundaries, with the constant pressure and temperature corresponding to given stagnation conditions. Vacuum outflow conditions were used in all of the computations shown next.

The convergence study has been performed for a nitrogen flow and the length of the plenum portion of the computational domain varying from 4 to $8L$. Comparison of the axial velocity and pressure profiles along the slot centerline are shown in Figs. 4 and 5, respectively. The slot entrance is located at $X = 0.005$ m. The difference between the three cases is within the statistical uncertainty of the computations, which was a few percent for flowfields and less than a percent for integral properties, such as mass flow and thrust. Because no visible influence of the computational domain size was observed when the subsonic chamber length was increased from $4L$ to $8L$, the value of $4L$ was used thereafter. A sensitivity study has also been performed with the downstream domain size

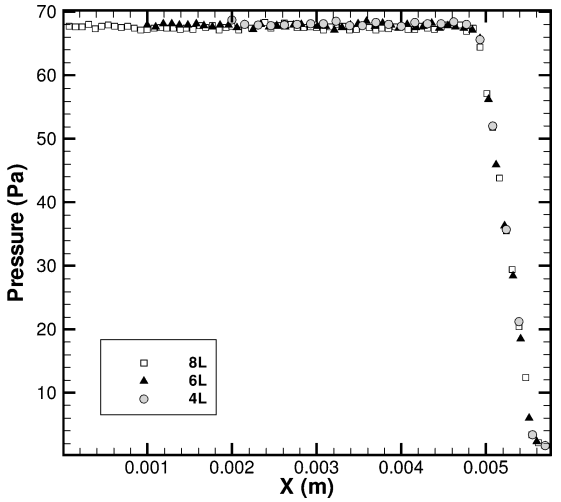

Fig. 5 Pressure profile along the axis of symmetry for different computational domains.

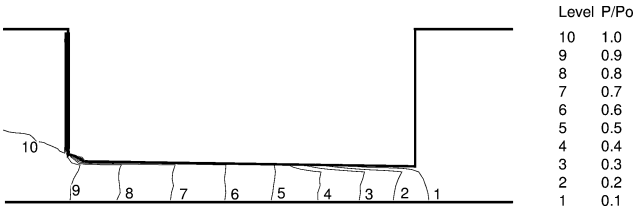

Fig. 6 Normalized pressure fields for $P_0 = 49$ Pa and the heater chip temperature of 300 K, area shown 750 × 250 μm.

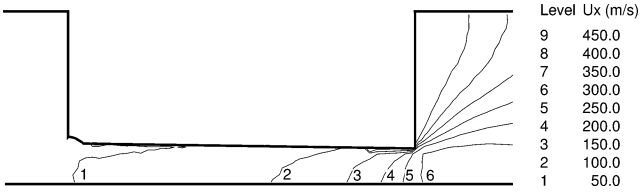

Fig. 7 Axial-velocity (m/s) fields for $P_0 = 49$ Pa and the heater chip temperature of 300 K, area shown 750 × 250 μm.

varied several times to obtain solutions free of the influence of the downstream domain. The downstream domain length of $18L$ was used in the computations discussed in the next section. The typical numbers of collision cells and simulated molecules are 50,000 and one million, respectively.

IV. Effects of Heater Chip Temperature and Stagnation Pressure on Flowfields

The FMMR will operate at an elevated heater chip temperature of about 573 K in order to achieve acceptable efficiency of the thruster. Because the Knudsen number will be about unity based on the slot width, the molecule exit velocity will be primarily determined by the surface temperature and is expected to be proportional to the square root of this temperature T_w. The mass flow is therefore expected to be proportional to the product of the gas density near the slot exit n_e and $\sqrt{T_w}$, whereas the thrust is proportional to $n_e T_w$.

The structure of the flow inside a single slot is shown in Fig. 6 for nitrogen propellant. The pressure values here are normalized by the plenum value. The computations showed that the impact of surface temperature on pressure is negligible—the variation is within 1%. The gas temperature near and inside the slot was found to be close to the surface temperature both for 300 and 573 K, whereas the gas density inside the slot normalized by the plenum value is not affected by the surface temperature.

However, the flow velocity changes significantly with temperature, as illustrated in Figs. 7 and 8. The velocity reaches 50 m/s

Table 1 FMMR performance in nitrogen: two-dimensional computations

P_0, Pa	T_w, K	Mass flow, kg/s	Thrust, N	Isp, s
49	300	$6.7975 \cdot 10^{-7}$	$3.0201 \cdot 10^{-4}$	45.29
49	400	$5.9912 \cdot 10^{-7}$	$3.0287 \cdot 10^{-4}$	51.53
49	500	$5.4257 \cdot 10^{-7}$	$3.0235 \cdot 10^{-4}$	56.80
49	573	$5.1239 \cdot 10^{-7}$	$3.0346 \cdot 10^{-4}$	60.37
69	300	$9.6524 \cdot 10^{-7}$	$4.3337 \cdot 10^{-4}$	45.77
69	400	$8.3901 \cdot 10^{-7}$	$4.2863 \cdot 10^{-4}$	52.08
69	500	$7.5192 \cdot 10^{-7}$	$4.2418 \cdot 10^{-4}$	57.51
69	573	$7.0806 \cdot 10^{-7}$	$4.2421 \cdot 10^{-4}$	61.07
95	300	$1.3343 \cdot 10^{-6}$	$6.0446 \cdot 10^{-4}$	46.18
95	400	$1.1502 \cdot 10^{-6}$	$5.9265 \cdot 10^{-4}$	52.52
95	500	$1.0299 \cdot 10^{-6}$	$5.8689 \cdot 10^{-4}$	58.09
95	573	$9.6222 \cdot 10^{-7}$	$5.8319 \cdot 10^{-4}$	61.78
139	300	$1.9982 \cdot 10^{-6}$	$9.1677 \cdot 10^{-4}$	46.77
139	400	$1.7075 \cdot 10^{-6}$	$8.9177 \cdot 10^{-4}$	53.24
139	500	$1.5112 \cdot 10^{-6}$	$8.7141 \cdot 10^{-4}$	58.78
139	573	$1.4081 \cdot 10^{-6}$	$8.6446 \cdot 10^{-4}$	62.58
185	300	$2.7053 \cdot 10^{-6}$	$1.2521 \cdot 10^{-3}$	47.18
185	400	$2.2717 \cdot 10^{-6}$	$1.1970 \cdot 10^{-3}$	53.71
185	500	$2.0041 \cdot 10^{-6}$	$1.1677 \cdot 10^{-3}$	59.39
185	573	$1.8527 \cdot 10^{-6}$	$1.1473 \cdot 10^{-3}$	63.12

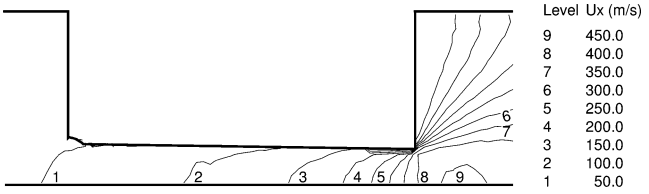

Fig. 8 Axial-velocity (m/s) fields for $P_0 = 49$ Pa and the heater chip temperature of 573 K, area shown 750 × 250 μm.

inside the slot for 300 K case and upstream from the slot entrance for 573 K. The magnitude of the difference increases toward the slot exit and reaches over 100 m/s for the gas that leaves the slot (280 m/s for 300 K and almost 400 m/s for 573 K). This increase is nearly proportional to $\sqrt{T_w}$. Note that this proportionality can be expected for a long channel and near free-molecule flow; it is not obvious however for a slot with a finite length-to-thickness ratio of five, a Knudsen number of one, and $T = 300$ K. In the latter case there are two more contributing sources that complicate the analysis. First, molecules that come directly from the plenum without interacting with the slot walls increase the average velocity. Second, molecules that collide with other molecules generally decrease the velocity. If these sources are small compared to the main surface-generated source, or if they compensate each other, the velocity will be proportional to $\sqrt{T_w}$.

The computations performed for a stagnation pressure of 185 Pa have shown that an almost four-fold increase in pressure does not change the flow pattern. Although the molecular collisions inside the slot become likely as the mean free path becomes one-fourth of the slot width, the length of the slot is still sufficient to increase velocities of most particles coming through it. Also, the average exit velocities are almost identical for 49 and 185 Pa.

V. FMMR Performance and Comparison with Experimental Data

Consider now the performance characteristics of a single FMMR slot for various gas pressures and surface temperatures. The mass flow, thrust, and specific impulse are listed in Table 1 for a nitrogen flow. For all cases, the mass flow is nearly inversely proportional to $\sqrt{T_w}$. Some deviation from the proportionality is related primarily to the effect of gas-gas collisions inside the slot. There is also some finite number of molecules, especially for lower pressures, that come directly from the plenum without interacting with heated slot walls.

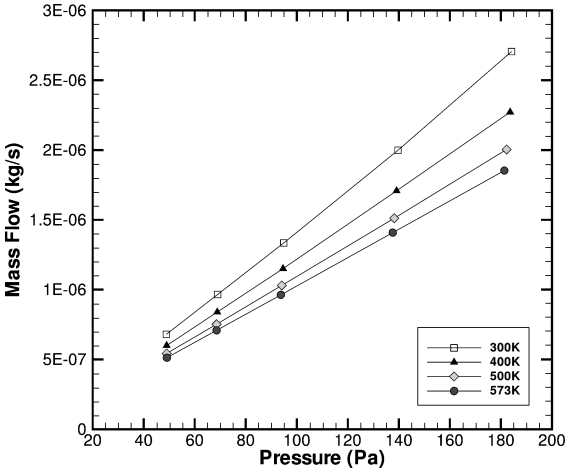

Fig. 9 Mass flow of nitrogen vs computed plenum pressure for different heater chip temperatures.

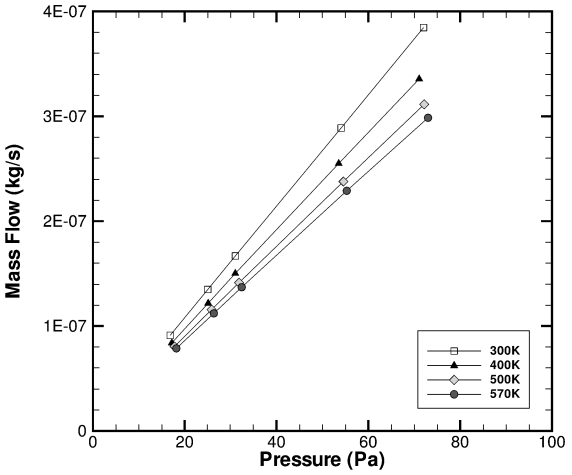

Fig. 10 Mass flow of helium vs computed plenum pressure for different heater chip temperatures.

There is a relatively weak dependence of thrust on surface temperature because the gas density is inversely proportional to T_w throughout the slot, whereas the velocity squared is proportional to T_w. The thrust does not change with T_w for $P_0 = 49$ Pa. At $P_0 = 185$ Pa, however, there is a 10% thrust degradation between heater chip temperatures of 300 and 573 K. The specific impulse slightly increases with pressure, with I_{sp} for $P_0 = 185$ Pa about 4% higher than for $P_0 = 49$ Pa. The ratio of specific impulse values for 573 K to that for 300 K does not depend on pressure and is equal to about 1.34. This is somewhat lower than the theoretical free-molecular value of 1.38.

The numerical results for the mass flow as a function of pressure at different heater chip temperatures are presented in Figs. 9 and 10 for two propellants, nitrogen and helium. The DSMC values of stagnation pressure are used here, obtained as an average over all plenum cells. It is clearly seen that in the considered range of pressures the mass flow is nearly linear for all surface temperatures, $\dot{m} \approx C p_0$. The proportionality coefficient C is in turn inversely proportional to T_w.

At a fixed pressure, the mass flow strongly depends on the geometry of the heater chip. Although the shape of the FMMR slot cross sections is known qualitatively, the uncertainty in the actual dimensions, primarily entrance and exit width, is no better than 10%. Moreover, the dimensions can differ for different slots. These uncertainties prevent direct comparison of mass flow and thrust computed as functions of pressure with the corresponding experimental data. They are however expected to be a minor issue for comparison of thrust vs mass flow because the pressure dependence is weak in this case.

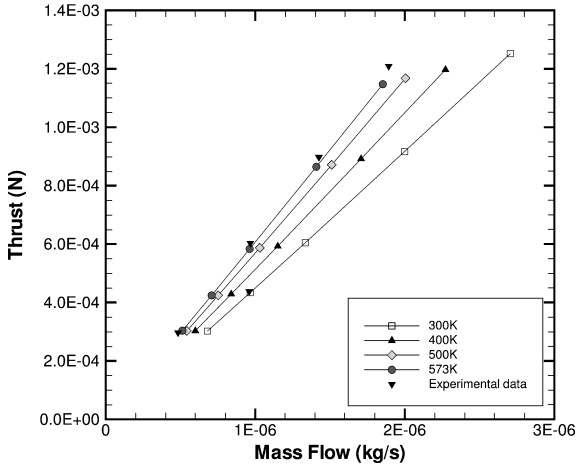

Fig. 11 Thrust force in nitrogen vs mass flow rate for different heater chip temperatures: comparison with experimental data.

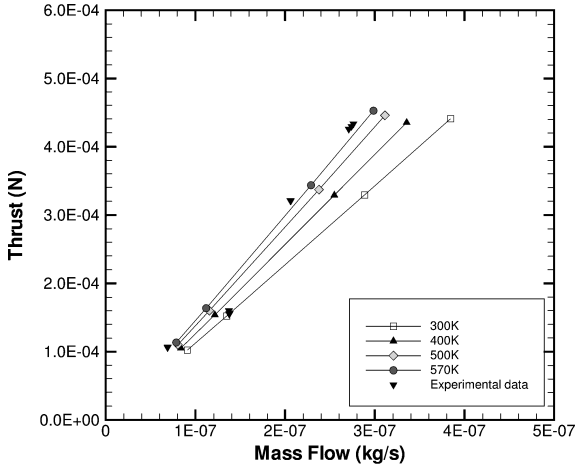

Fig. 12 Thrust force in helium vs mass flow rate for different heater chip temperatures: comparison with experimental data.

Comparison of the calculated force with the experimental data[10] at 573 K for nitrogen and 300 and 573 K for helium is given in Figs. 11 and 12. As expected, both experimental and numerical thrust values exhibit nearly linear dependence vs mass flow. For nitrogen, the computed thrust is about 2% lower than the experimental values. This is attributed primarily to the impact of the plume molecules backscattered to the outer surface of the heater chip. Such molecules increase the total thrust force, and such an impact is underestimated because of the limitations of the two-dimensional numerical statement of the problem. The impact of the backscattered molecules is larger for helium because of its lower mass and larger backscattering; as a result, the difference between the computed and measured thrust values is somewhat larger for this gas.

VI. Three-Dimensional Modeling of the Plenum Flow

The modeling of the FMMR plume flow was performed in two steps. First, the flow inside the plenum and in the near field of the plume was calculated. The numbers of simulated molecules and collision cells in these computations were about 3 million and 0.6 million, respectively. The results were used to specify gas parameters at a starting surface parallel to the outer heater chip plane and 0.5 mm downstream. The starting surface is utilized in the subsequent modeling of the plume interaction and impingement. Because water vapor has been identified as the ideal FMMR propellant, it was used in these computations.

The results of plenum flow modeling are presented in Figs. 13 and 14, where the pressure and temperature fields are shown respectively for $P_0 = 306.5$ Pa and heater chip temperature of 573 K

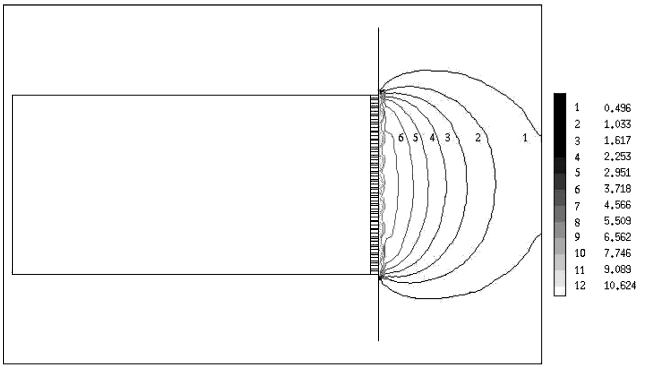

Fig. 13 Pressure (Pa) field inside the plenum for $P_0 = 306.5$ Pa and $T_w = 573$ K, area shown 33 × 23 mm.

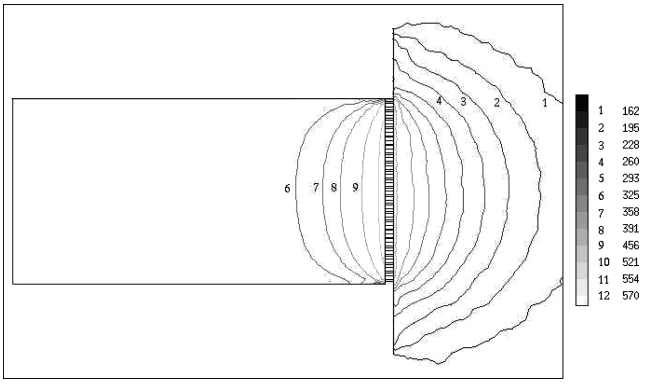

Fig. 14 Translational temperature field inside the plenum for $P_0 = 306.5$ Pa and $T_w = 573$ K, area shown 33 × 23 mm.

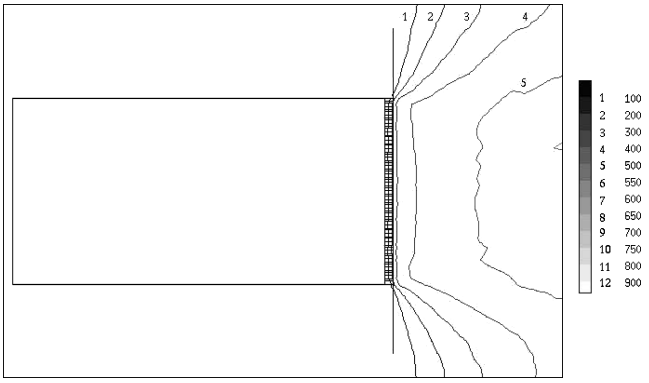

Fig. 15 Flow velocity for $P_0 = 306.5$ Pa and $T_w = 300$ K, area shown 33 × 23 mm.

at the symmetry plane. The figure also illustrates the geometry of the plenum. The gas is supplied through a 6.35-mm tube located at the top left part of the plenum. No significant pressure gradients were observed inside the plenum, with pressure decreasing by less than 1% from the inflow tube to the heater chip. The gas temperature increases from the inflow value of 300 to 573 K in the heated slot region. Note that the increase occurs in the downstream quarter of the plenum, and the gas temperature is significantly less in the regions close to the top and bottom plenum walls that are kept at 300 K. The gas temperature is constant inside the slots and decreases rapidly in the expansion region.

The flow velocity in the direction perpendicular to the heater chip is shown in Figs. 15 and 16 for two heater chip temperatures. Similar to the two-dimensional case, the velocity is higher for 573 K; however, the difference is somewhat smaller for the three-dimensional flow. Note also that multiple jets result in velocity isolines being parallel to the heater chip plane outside the chip; this flow pattern propagates more than 2 cm downstream.

Table 2 FMMR performance for water vapor: three- and two-dimensional simulations

P_0, N/m^2	Wall temperature, K	Case	Mass flow, kg/s	Thrust, N	Isp, s
61.3	300	Three-dimensional	$4.9124 \cdot 10^{-7}$	$2.5970 \cdot 10^{-4}$	53.89
61.3	300	Analytic	$4.2869 \cdot 10^{-7}$	$2.7607 \cdot 10^{-4}$	65.71
61.3	570	Two-dimensional	$4.3984 \cdot 10^{-7}$	$3.1847 \cdot 10^{-4}$	73.81
61.3	570	Three-dimensional	$4.0872 \cdot 10^{-7}$	$2.8756 \cdot 10^{-4}$	71.72
306.5	300	Three-dimensional	$4.0872 \cdot 10^{-6}$	$1.0957 \cdot 10^{-3}$	54.40
306.5	300	Analytic	$2.1435 \cdot 10^{-6}$	$1.3804 \cdot 10^{-3}$	65.71
306.5	570	Two-dimensional	$2.0655 \cdot 10^{-6}$	$1.5605 \cdot 10^{-3}$	77.01
306.5	570	Three-dimensional	$1.8112 \cdot 10^{-6}$	$1.3034 \cdot 10^{-3}$	73.35

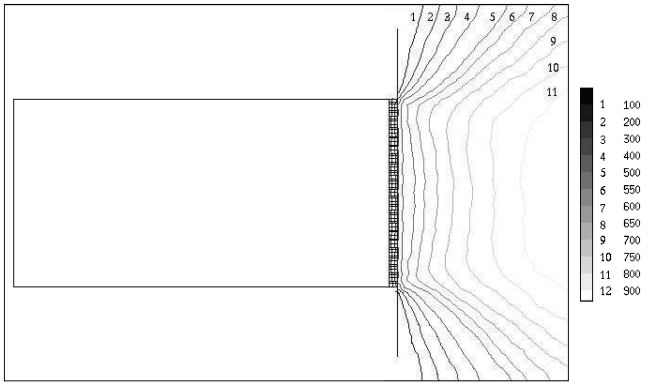

Fig. 16 Flow velocity for $P_0 = 306.5$ Pa and $T_w = 573$ K, area shown 33 × 23 mm.

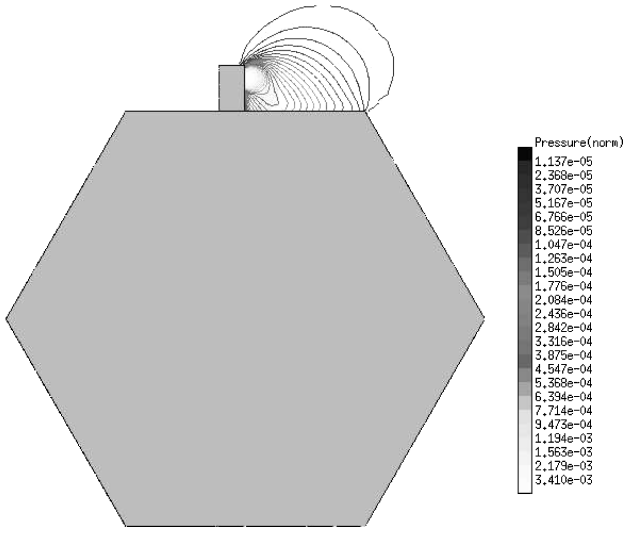

Fig. 17 Normalized pressure field for $P_0 = 306.5$ Pa and $T_w = 573$ K.

Let us now examine the impact of heater chip temperature on the FMMR performance. The performance properties are listed in Table 2 for two plenum pressures and two heater temperatures using a water propellant. In contrast to the previous two-dimensional runs, the full three-dimensional modeling results in a simultaneous decrease in the mass flow and increase in thrust when the temperature increases from 300 to 573 K. Note that the decrease in the mass flow is lower than the the square root of the temperature ratio. This behavior is attributed to the impact of the cold plenum walls. The gas is colder than T_w in the downstream corners of the plenum, which in turn causes the larger number density and mass flows at these locations.

Comparison of three-dimensional results with the corresponding two-dimensional parameters (rectangular slots were used in these two-dimensional computations to make comparison meaningful) shows that the complex three-dimensional flow in the plenum results in significantly, about 10%, lower values of both mass flow and thrust. The specific impulse however is close in two- and three-dimensional computations. Generally, it increased by a factor of 1.34 when the heater chip temperature was increased from 300 to 573 K, which is the same as in two-dimensional modeling for helium and nitrogen propellants.

Analytic predictions obtained using the free-molecular analysis of Ref. 10 are also given in Table 2. These estimates were calculated using the assumption that the gas pressure near the FMMR slot entrances is close to the stagnation value, whereas the gas temperature is close to the slot temperature of 573 K. This assumption is reasonable at the range of pressures considered, although it will fail for lower stagnation pressures. The analytic mass flows are within 4% of the corresponding two-dimensional DSMC values, whereas the analytic values of thrust are closer to the three-dimensional DSMC values. As the result, the analytic specific impulse is over 10% lower than that computed with the DSMC method, both two- and three-dimensional.

VII. Modeling of the Plume Expansion Flow

The modeling of the plume expansion and impingement on the spacecraft surface has been performed for the four three-dimensional cases shown in Table 2. The preceding computations were used to determine parameters for the ellipsoidal distribution function at a starting surface located immediately downstream of the heater chip. Two possible locations of the FMMR were examined, the one shown in Fig. 2 and another one with the FMMR positioned close to the edge of the cylinder panel. The numbers of molecules and cells in these computations were about 5 million and 1.2 million, respectively.

The general flowfield structure for the first location is shown in Fig. 17, where the pressure field normalized by the stagnation value is presented in the plane perpendicular to the heater chip surface and coming through the chip center. Note that the normalized pressure only weakly depends on the plenum pressure when decreased from 306.5 to 61.3 Pa and heater chip temperature when changed from 573 to 300 K. There is a clearly visible interaction region between the plume and the top surface of the satellite approximately 3 cm downstream from the heater chip plane. The pressure there is about 50 times higher than that in the corresponding region above the FMMR.

Figure 18 presents the mass flux of water molecules on the surface of the spacecraft. The important conclusion here is that the plume molecules interact only with the top panel of the spacecraft. No molecular flux was registered on the other panels. This means that molecular flux from the plume will be smaller on these surfaces than that from the freestream in low Earth orbit. The mass flux on the top surface is significant both for contamination and thrust degradation.

The distribution of the mass flux over the spacecraft surface for the second tested location of the FMMR is shown in Fig. 19. There are still water molecules that collide with the cylinder panel where the FMMR is attached, mostly near the panel edge; however, this number is 98% smaller than that for the first considered location. Molecules also reach the adjacent panel of the hexagonal cylinder, and their flux is 85% higher than that for the panel where the FMMR is attached.

Table 3 Thrust degradation of FMMR located on center of panel

P_0, Pa	Wall temperature, K	Surface mass flow, kg/s	Surface force x, N	Surface force y, N	Net thrust x	Net moment, N · m
61.3	300	$1.6628 \cdot 10^{-7}$	$-8.7785 \cdot 10^{-5}$	$-5.6008 \cdot 10^{-5}$	$1.7191 \cdot 10^{-4}$	$2.91 \cdot 10^{-5}$
61.3	573	$1.3623 \cdot 10^{-7}$	$-9.7307 \cdot 10^{-5}$	$-6.0045 \cdot 10^{-5}$	$1.9026 \cdot 10^{-4}$	$3.24 \cdot 10^{-5}$
306.5	300	$7.5071 \cdot 10^{-7}$	$-3.8529 \cdot 10^{-4}$	$-2.7352 \cdot 10^{-4}$	$7.1046 \cdot 10^{-4}$	$1.18 \cdot 10^{-4}$
306.5	573	$6.4807 \cdot 10^{-7}$	$-4.5280 \cdot 10^{-4}$	$-3.0385 \cdot 10^{-4}$	$8.5057 \cdot 10^{-4}$	$1.14 \cdot 10^{-4}$

Table 4 Thrust degradation of FMMR located at edge of panel

P_0, Pa	Wall temperature, K	Surface mass flow, kg/s	Surface force x, N	Surface force y, N	Net thrust x	Net moment, N · m
61.3	300	$4.7786 \cdot 10^{-9}$	$-2.6883 \cdot 10^{-6}$	$-8.5304 \cdot 10^{-6}$	$2.5701 \cdot 10^{-4}$	$4.72 \cdot 10^{-5}$
61.3	573	$2.9353 \cdot 10^{-9}$	$-2.7986 \cdot 10^{-6}$	$-8.4020 \cdot 10^{-6}$	$2.8476 \cdot 10^{-4}$	$5.24 \cdot 10^{-5}$
306.5	300	$3.5330 \cdot 10^{-8}$	$-1.4756 \cdot 10^{-5}$	$-5.4401 \cdot 10^{-5}$	$1.0810 \cdot 10^{-3}$	$1.96 \cdot 10^{-4}$
306.5	573	$2.4430 \cdot 10^{-8}$	$-1.5821 \cdot 10^{-5}$	$-5.3402 \cdot 10^{-5}$	$1.2876 \cdot 10^{-3}$	$2.35 \cdot 10^{-4}$

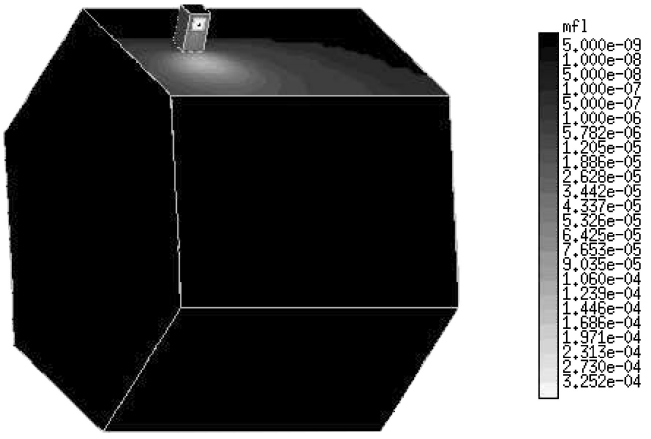

Fig. 18 Surface mass flux (kg/m^2) for $P_0 = 306.5$ Pa and $T_w = 573$ K.

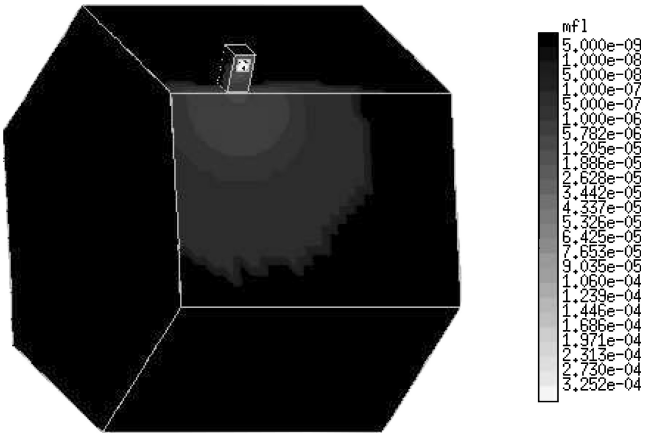

Fig. 19 Surface mass flux (kg/m^2) (right) for $P_0 = 306.5$ Pa and $T_w = 573$ K.

Consider now the impact of the FMMR parameters and location on the integral surface parameters. Tables 3 and 4 show the values of the total surface mass flow for different flow cases. Generally, the amount of plume molecules that hit the surface is nearly proportional to the plenum pressure. Because the mass flow through the heater chip decreases with temperature at fixed pressures, the potential for surface contamination by plume molecules is also lower in this case. This decrease is especially significant for the second location of the FMMR.

Tables 3 and 4 also give the total surface forces in X direction (the direction of the FMMR thrust) and Y direction. For the first location of the FMMR, both X and Y components of the surface forces decrease with the FMMR temperature, thus degrading the net force. The net force column of the table represents the X component of the total force during the operation of FMMR, obtained as a sum of the thrust force (see Table 2) and the surface force. The important conclusion here is that for the first FMMR location the surface force is comparable in magnitude with the thrust force, which results in about 30% thrust degradation as a result of the plume-surface interaction.

When the FMMR is located at the edge of the cylinder panel, the surface force is only about 1% of the thrust force, and the primary factors that contribute to the despinning capability of the FMMR are the thrust force, the direction of the plume, and the arm length. The net despinning moment values are presented in the last column of Tables 3 and 4. For both FMMR locations, the temperature increase from 300 to 570 K results in the net moment increase of 10% for lower pressure and 20% for higher pressure, at a significantly lower mass flow. Most importantly, the second FMMR location is characterized by a 60% higher net moment than the first location. Note that tilting the FMMR clockwise in the second location will increase the contribution of the thrust force to the despinning moment, but at the same time is expected to significantly increase the moment degrading surface forces.

VIII. Conclusions

The gas flow in a free-molecule microresistojet is studied numerically with the direct-simulation Monte Carlo method. A two-dimensional flow of nitrogen and helium is modeled through a single heater slot for a qualitatively accurate slot geometry. The results were obtained for a range of plenum pressures from 50 to 200 Pa and heater chip temperatures from 300 to 573 K.

The thrust was found to be a weak function of the surface temperature, whereas the mass flow was inversely proportional to the square root of the temperature. The results were compared with available experimental data for thrust vs mass flow. A reasonable agreement of numerical and experimental data was observed. The computed specific impulse was about 2% lower than that of experimental data for nitrogen and about 4% for helium. The difference is attributed to the impact of the backscattered plume molecules that act toward increasing thrust; this impact is not properly accounted for in the two-dimensional modeling.

A full three-dimensional modeling of the FMMR geometry has been performed for water vapor in two steps. First, the flow in the plenum was modeled. A significant impact of the cold side walls was found on the FMMR performance parameters compared to the two-dimensional computations. In three-dimensions, the thrust significantly increases with temperature. The mass flow decreases with temperature, but the decrease is less significant than in two-dimensions. At the same time, the specific impulse increases with temperature by a factor of 1.34 when the wall temperature increases from 300 to 573 K both for two and three dimensions.

Second, the FMMR plume flow was computed using a starting surface generated from the plenum simulation. Two locations of the

FMMR were examined—the center of a cylinder panel and the edge of the panel. For the first location, the potential for contamination is important only for the panel of the satellite where the FMMR is installed. For the second location, both the FMMR and the adjacent panels are affected by water molecules, but to an order of magnitude smaller extent than for the first location. For the first location, the surface force caused by the plume-surface interaction is large compared to the thrust force, and the thrust degradation can be as large as 30%. For the second location, the surface-related degradation is only about 1% of the thrust force. The despinning moment is over 60% larger for the second location.

Acknowledgment

This work was supported in part by the Propulsion Directorate of the Air Force Research Laboratory at Edwards Air Force Base, California. The authors thank Taylor Lilly and Riki Lee who provided experimental data for comparison.

References

[1]Ketsdever, A. D., "System Considerations and Design Options for Microspacecraft Propulsion Systems," *Micropropulsion for Small Spacecraft*, edited by M. Micci and A. Ketsdever, Progress in Astronautics and Aeronautics, Vol. 187, AIAA, Reston, VA, 2000, Chap. 4.

[2]Reed, B. D., de Groot, W., and Dang, L., "Experimental Evaluation of Cold Flow Micronozzles," AIAA Paper 2001-3521, July 2001.

[3]Hitt, D. L., Zakrzwski, C. M., and Thomas, M. A., "MEMS-Based Satellite Micropropulsion via Catalyzed Hydrogen Peroxide Decomposition," *Smart Materials and Structures*, Vol. 10, No. 6, 2001, pp. 1163–1175.

[4]London, A. P., Epstein, A. H., and Kerrebrock, J. L., "High-Temperature Bipropellant Microrocket Engine," *Journal of Propulsion and Power*, Vol. 17, No. 4, 2001, pp. 780–787.

[5]Ketsdever, A., Green, A., Muntz, E. P., and Vargo, S., "Fabrication and Testing of the Free Molecule Micro- Resistojet: Initial Results," AIAA Paper 2000-3672, July 2000.

[6]Ketsdever, A. D., Lee, R. H., and Lilly, T. C., "Performance Testing of a Microfabricated Propulsion System for Nanosatellite Applications," *Journal of Micromechanics and Microengineering*, Vol. 15, No. 12, 2005, pp. 2254–2263.

[7]Ivanov, M. S., Markelov, G. N., and Gimelshein, S. F., "Statistical Simulation of Reactive Rarefied Flows: Numerical Approach and Applications," AIAA Paper 98-2669, June 1998.

[8]Ivanov, M. S., and Rogasinsky, S. V., "Analysis of the Numerical Techniques of the Direct Simulation Monte Carlo Method in the Rarefied Gas Dynamics," *Soviet Journal of Numerical Analysis and Mathematical Modelling*, Vol. 3, No. 6, 1988, pp. 453–465.

[9]Bird, G. A., *Molecular Gas Dynamics and the Direct Simulation of Gas Flows*, Clarendon Press, Oxford, England, UK, 1994, Chap. 2.

[10]Lee, R. H., Lilly, T. C., Muntz, E. P., and Ketsdever, A. D., "Free Molecule Microresistojet: Nanosatellite Propulsion," AIAA Paper 2005-4073, July 2005.

[11]Cercignani, C., *Rarefied Gas Dynamics: from Basic Concepts to Actual Calculations*, Cambridge Univ. Press, Cambridge, England, UK, 2000, Chap. 4.